Available online at www.sciencedirect.com

ScienceDirect

Materials Today: Proceedings XX (2016) XXX–XXX

materialstoday: PROCEEDINGS

www.materialstoday.com/proceedings

PMME 2016

Structural, morphological, photoluminescence and electrical characterization of aluminum doped ZnO phosphors for solar cell applications☆

Swati Bishnoi[a,b], B. Rajesh [a,b], G. Swati[a,b], Vishnu Vikesh Jaiswal[a], Mukesh Sahu[a], Paramjeet Singh[a] and D. Haranath[a,*]

[a]*CSIR-National Physical Laboratory (NPL), Dr. K. S. Krishnan Road, New Delhi – 110012, India*
[b]*Academy of Scientific and Innovative Research (AcSIR), CSIR-NPL Campus, New Delhi- 110012, India*

Abstract

We report synthesis of highly luminescent and n-type conducting aluminum doped ZnO (AZO) phosphors using flux-free solid-state reaction technique followed by casting of thin films. The precursor powders were pelletized and fired at 1000ºC (AZO-1). In another typical case, 2-stage sequential firing has been adapted at 1000ºC followed by 1200ºC (AZO-2) in a flowing O_2 gas environment. The stabilization (dwell) time has been fixed as 2 hours for all temperatures of firing in the furnace. After firing at 1200°C, a new cubic phase (zinc aluminate) has been observed in the lattice along with the wurtzite ZnO phase. The microstructure analysis was substantiated with Rietveld refinement of the diffraction data of AZO-1 and AZO-2 samples. The photoluminescence (PL) measurements revealed that both AZO-1 and AZO-2 exhibited green (~523 nm) PL under UV (375 nm) excitation, with emission intensity of AZO-1 comparatively higher than that of AZO-2 sample. Moreover, the measurement of electronic transport properties of the AZO-1 and AZO-2 samples exposed their n-type behavior, with slightly lower electrical resistivity of AZO-1 (4.7×10^{-3} Ω-m) as compared to AZO-2 (3×10^{-3} Ω-m) at 700 K temperature. The AZO samples have been used as target materials for transparent thin film deposition on quartz substrate, thus proving it to be ideal materials for solar cell applications.

* Corresponding author. Tel.: +91-11-4560 9385; fax: +91-11-4560 9310.
E-mail address: haranath@nplindia.org

2214-7853
Selection and Peer-review under responsibility of International Conference on Processing of Materials, Minerals and Energy (July 29th – 30th) 2016, Ongole, Andhra Pradesh, India.

Selection and Peer-review under responsibility of International Conference on Processing of Materials, Minerals and Energy (July 29th – 30th) 2016, Ongole, Andhra Pradesh, India.

Keywords: Photoluminescence, SEM, XRD, Seebeck, resistivity, solar cells

1. Introduction:

Zinc oxide (ZnO) is a well-known wide band gap semiconductor and is attaining remarkable consideration in various fields related to chemistry and physics due to its commendable physical and chemical properties. Moreover, ZnO has a wide variety of applications in various technological areas such as optoelectronics, photonics, solar cells, and memory devices, optical devices such as light emitting diodes, laser diodes [1, 2], solid-state lighting, rubber industries, ceramic glazes etc. [3, 4, 5]. Recently, electronic properties of ZnO have been explored for their applications in sensors [6] and varistors [7]. Pristine ZnO shows n-type conductivity due to the native defects such as oxygen vacancies, zinc interstitials etc. present in the lattice [8-10]. But the conductivity of pristine ZnO is thermally unstable. Due to which researchers adapt the procedure of doping of group III elements (B^{3+}, Al^{3+}, Ga^{3+}, and In^{3+}) in ZnO, wherein Zn^{2+} ions can be substituted by these ions [11-13] that generates extra electrons and improves optical, electrical and thermal stability of ZnO. Al^{3+} is most commonly used dopant from group III elements owing to its small ionic radius (67.5 pm), comparable to Zn^{2+} (88 pm) and cost-effectiveness. The substitution of Zn^{2+} ions by Al^{3+} improvises the electrical conductivity and results in high quality samples with significantly low resistivity.

Aluminium doped ZnO (AZO) compounds have also shown conductivity enhancement as compared to pristine ZnO samples, along with improved transparency [14, 15]. Moreover, it has been reported that in Al-doped ZnO thin films, band gap increases as compared to pristine ZnO. This increase in band gap can be utilized in optical applications in the visible range [16]. Studies for structural analysis of Al doped ZnO has also been carried out [17]. Tunable infrared absorption and visible transparency in Al doped ZnO have also been reported [18]. However, very few reports are available regarding investigation of luminescent and thermoelectric properties of thin films for solar cells application.

In this article, we report synthesis of Al (5% wt.) doped ZnO by flux-free solid-state route, the precursors were mixed thoroughly and pelletized, initial firing of the pellet was carried at 1000ºC (AZO-1), followed by subsequent refiring at 1200ºC (AZO-2) in oxygen environment. The stabilization (dwell) time has been fixed as 2 hours for all temperatures of firing in the furnace. The structural and optical properties of pristine ZnO, AZO-1 and AZO-2 have been compared. Both AZO-1 and AZO-2 exhibits green emission (~523 nm) under UV excitation (375 nm), but the emission intensity of AZO-1 is higher as compared to AZO-2 sample. We have done Reitveld refinement of diffraction data of pristine ZnO, AZO-1 and AZO-2 samples. The Reitveld analysis of AZO-2 revealed formation of new cubic phase of zinc aluminate along with wurtzite phase in contrast to pristine ZnO and AZO-1 samples, which exhibited only wurtzite phase. Electronic transport properties such as resistivity and Seebeck coefficient explored n-type conductivity in both AZO-1 and AZO-2, with AZO-2 having higher electrical resistivity than AZO-1 attributed to the cubic phase generation. The pellet of AZO samples have been used for transparent (>80% in visible region) thin film deposition on quartz substrate, proving a potential candidate for solar cell applications.

2. Materials and Methods

All the samples were synthesized by a facile solid-state reaction technique. ZnO and Al precursor materials were mixed thoroughly pelletized and fired at 1000ºC in air atmosphere (AZO-1). Some of the samples were refired at 1200ºC in oxygen atmosphere. The stabilization (dwell) time has been fixed as 2 hours for all temperatures of firing in the furnace. The X-ray powder diffraction (XRD) of the sample was performed by Rigaku miniflex X-ray diffractometer using the principle of Bragg Brentano Geometry, with Cu-Kα radiation (1.54Å). The morphology of the AZO samples was analyzed using a LEO 440 PC digital scanning electron microscope (SEM). Time resolved photoluminescence (TRPL) decay was measured using Edinburgh Photoluminescence spectrometer (FLSP920)

Instrument. The n-type conductivity of the AZO-1 and AZO-2 sample was confirmed by measuring the thermoelectric or Seebeck coefficient (S) of the sample, calculated using the formula $S = \Delta V/\Delta T$, where ΔV is the thermo-emf produced across the sample due to the temperature difference ΔT. Thermal diffusivity measurements (Linseis, LFA 1000) were conducted on 12.7 mm diameter discs, and rectangular bars 10 mm x 3 mm x 3 mm were used for electrical transport measurements (Ulvac, ZEM 3) in the temperature range from room temperature to 750 K. The (AZO-1) sample pellet was used as a target for thin film deposition on quartz substrate. The deposition was carried out in oxygen atmosphere (O_2 pressure: 1 x 10^{-2} Torr) by maintaining the quartz substrate temperature at 800°C. Transparency of AZO film was measured using Avantes UV-VIS-NIR spectrometer.

3. Results and discussion

X-Ray Diffraction (XRD) technique was employed for phase characterization of pristine and Aluminium (Al) doped ZnO (AZO) samples. The XRD spectra of pristine ZnO, (AZO-1) and (AZO-2) samples are shown in Fig.1. The XRD of pristine ZnO and (AZO-1) sample are in good agreement with data corresponding to "wurtzite hexagonal" phase of ZnO (JCPDS Card No. 36-1451), which indicates that in AZO-1 sample, the doping of Al does not affect the wurtzite structure of ZnO but (AZO-2) sample exhibits some low intensity extra peaks owing to the formation of new phase.This is due to the facilitation of forming high temperature cubic phase of zinc aluminate above 1000°C

$$ZnO + xAl^{3+} \xrightarrow{1000^{\circ}C} Zn_{1-x}^{2+}\, Al_x^{3+}O + xZn^{2+}$$

$$ZnO + Al_2O_3 \xrightarrow{1200^{\circ}C} Zn_{1-x}^{2+}\, Al_x^{3+}O + xZn^{2+} + ZnAl_2O_4$$

The structural refinement of all the samples i.e., pure ZnO, (AZO-1) and (AZO-2) was done by using Rietveld full-profile analysis method, (Fig.1, 2 &3) which revealed that the sample ZnO and AZO-1 are single-phase crystallized in an wurtzite structure, the lattice constants are shown in Table 1. In AZO-2 the additional peaks at 31.2°, 36.75°, 59.3°, 65.3° were observed, corresponding to (220), (311), (511) and (440) diffraction planes of face-centered cubic spinel-structured $ZnAl_2O_4$ [19,20]. The cubic phase was not observed in pristine ZnO and AZO-1 sample. This implies the coexistence of two phases in high temperature fired AZO-2 sample which are ZnO: Al (wurtzite) and $ZnAl_2O_4$ (cubic). The lattice parameters (a,b,c) of the pristine ZnO, AZO-1 and AZO-2 samples are shown in Table 1. The a, b, c values of the AZO-1 sample have shown decreasing tendency as compared to the pristine ZnO sample, this can be due to the fact that the Zn atoms are replaced by the Al atoms and ionic radius of the cation Al^{3+} (53 pm) is smaller than Zn^{2+} cation (74 pm) hence, with increasing substitution of Zn with Al, lattice parameters a, b, c are decreasing owing to the lattice contraction, hence confirming that Al has been successfully doped in the lattice. In AZO-2 sample two phases [wurtzite-ZnO/ZnO-Al] and [cubic-$ZnAl_2O_4$] are observed, this could be due to the fact that at high temperature Al in presence of oxygen forms another minor phase $ZnAl_2O_4$.

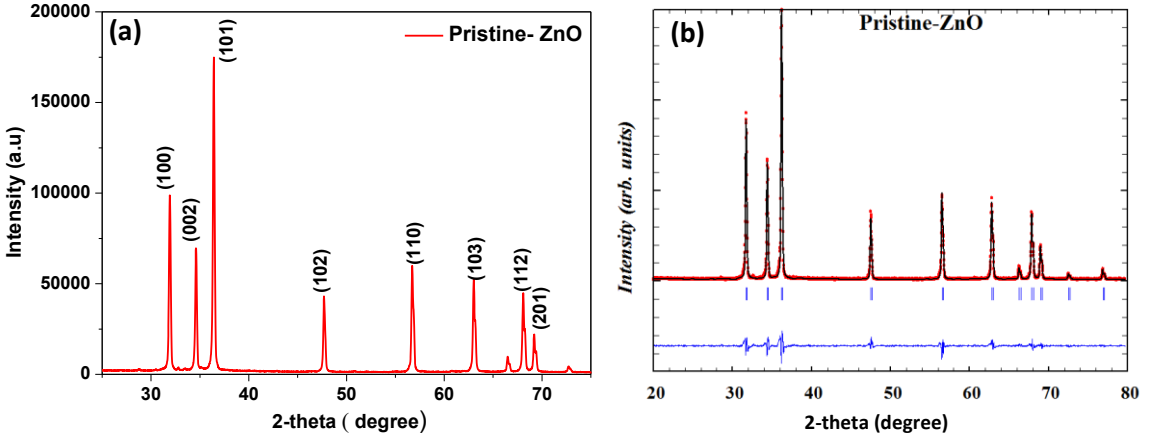

Fig.1. (a) XRD pattern of Pristine ZnO sample (b) Rietveld refinement, (b) red and black lines represent the observed and fitted data, respectively. The blue line represents the difference between the observed and fitted data.

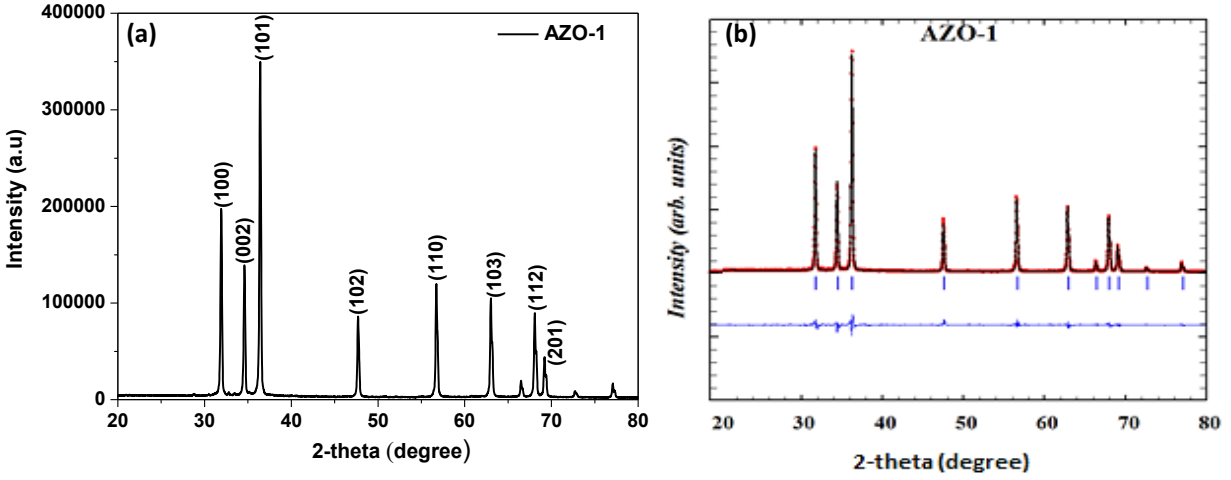

Fig.2. (a) XRD pattern of AZO-1 sample (b) Rietveld refinement of AZO-1, the red and black lines represent the observed and fitted data, respectively. The blue line represents the difference between the observed and fitted data.

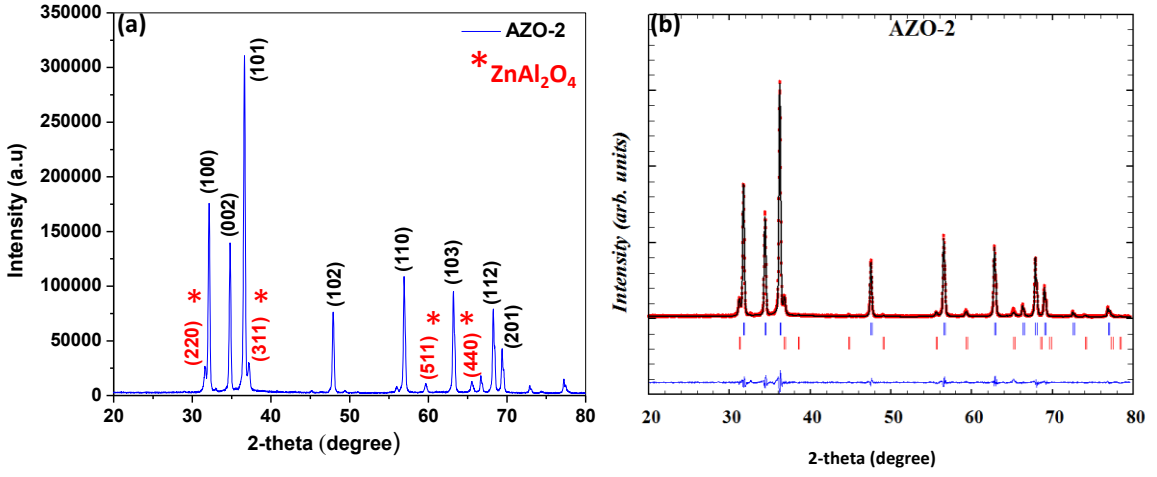

Fig.3. (a) XRD pattern of AZO-2 sample (b)Rietveld refinement of AZO-2, the red and black lines represent the observed and fitted data, respectively. The blue line represents the difference between the observed and fitted data.

Table 1. Table showing the lattice parameters of Pure ZnO, AZO-1 (ZnO: Al fired at 1000° C) and AZO-2 (ZnO: Al fired at 1200° C).

Lattice Parameters	**Pure ZnO**	**AZO-1**	**AZO-2**	
		ZnO:Al (95:5)	**ZnO: Al**	**$ZnAl_2O_4$**
		(Wurtzite)	**(Wurtzite)**	**(Cubic)**

a	3.253962 Å	3.2515 Å	3.2532 Å	8.0942 Å
b	3.253962 Å	3.2515 Å	3.2532 Å	8.0942 Å
c	5.208406 Å	5.2059 Å	5.2095 Å	8.0942 Å
Alpha	90°	90°	90°	90°
Beta	90°	90°	90°	90°
Gamma	120°	120°	120°	90°

The electron microscopy observations were carried out to check the morphology of AZO-1 and AZO-2 samples and are shown in Fig. 4(a-d). The SEM micrographs of AZO-1 {Fig.4(a)} and AZO-2 {Fig. 4(c-d)}, reveals the bulk characteristics of the samples with micron size particles. The particles have irregular morphology with truncated hexagonal shape. The high resolution SEM image of AZO-1 sample {Fig 4(b)}, shows the hexagonal boundaries of ZnO.

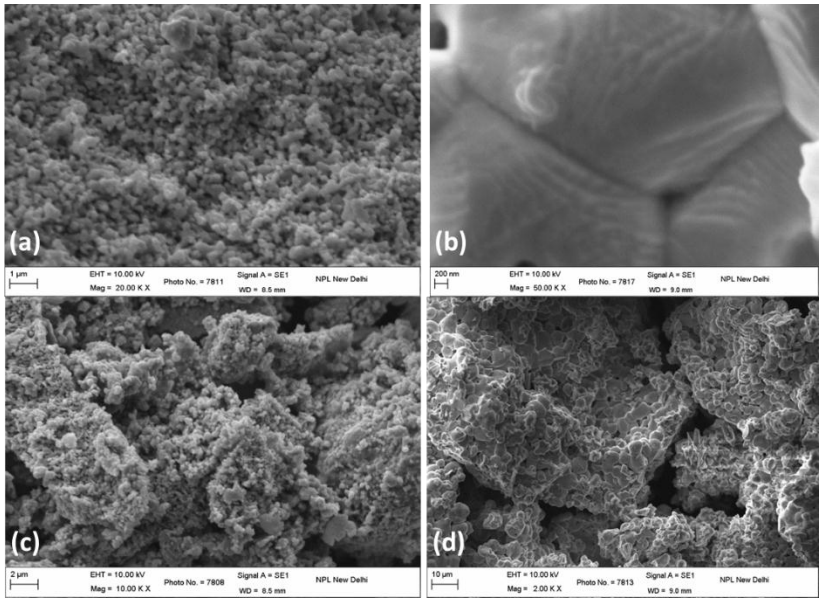

Fig 4.(a) and (b), SEM and HRSEM micrographs of AZO-1 samples; (c)-(d) SEM micrographs AZO-2 sample

The energy dispersive x-ray analysis (EDAX) confirmed the successful incorporation of Al in the ZnO lattice. The representative spectra EDAX of AZO-1 as shown in Fig. 5, shows a very weak signal for Al and a very prominent signal for Zn and O due to less doping % of Al.

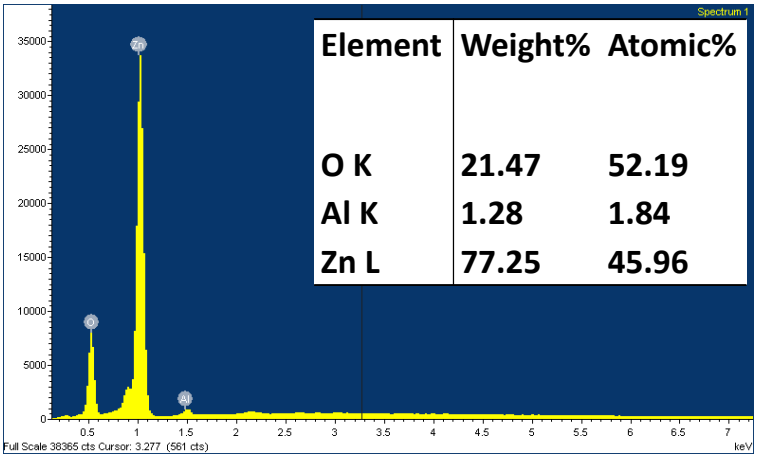

Fig 5. A representative EDAX spectra of AZO-1 sample showing successful doping of Al in ZnO lattice

The photoluminescence excitation and emission spectra of AZO-1 &AZO-2 samples are shown in Fig. 6(a-b), respectively. The samples are emitting green light (~523 nm) under UV (375 nm) excitation, the symmetric emission peak is centered around 523 nm, this is attributed to the several intrinsic and extrinsic defects (i.e. oxygen vacancies, zinc vacancies as well as donor-acceptor pairs) in ZnO [19, 20]. In AZO samples green emission can also be attributed to recombination between Al related donor level to some intrinsic acceptor levels or we can say green emission is observed due to recombination of electron-hole pair between conduction band and zinc vacancy acceptor center V_{Zn} or oxygen interstitials (O_i) [21-23]. According to previous reports, the Vzn acceptor level lies 0.3 eV above valence band [24] and O_i lies 0.4 eV above the valence band, so for green emission to be observed at ~523 nm in AZO sample the corresponding band gap is 2.37 eV. This implies that the Al^{3+} energy level might be located 0.65 eV below the conduction band for green emission to occur as shown in Fig 7(a). Moreover, the emission intensity of the AZO-1 sample is comparatively higher than the AZO-2 sample attributed to formation of zinc aluminate cubic phase and additional zinc vacancy V_{zn} in the latter due to firing at higher temperature in O_2 environment. The additional cubic phase zinc aluminate enhances non–radiative recombinations in the AZO-2 sample thus reducing the luminescence intensity.

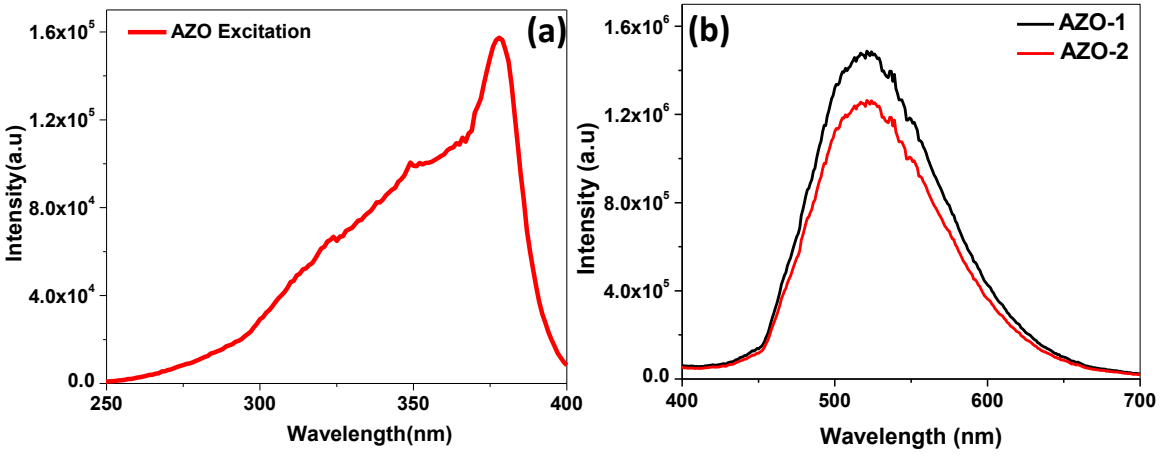

Fig 6.(a) PL Excitation spectra of AZO (b) Emission spectra of AZO-1 and AZO-2 samples

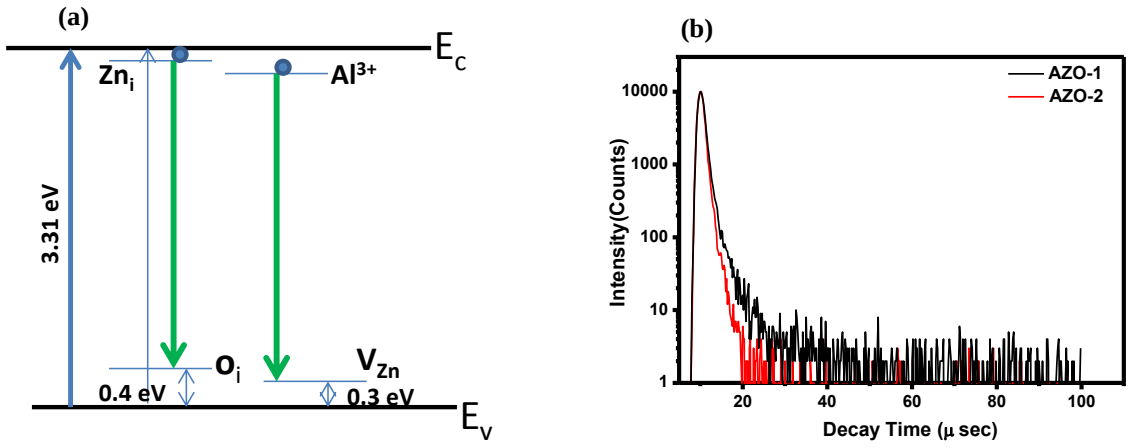

Fig. 7.(a) Energy level diagram showing mechanism of green emission in AZO (b) Time resolve PL decay curve of AZO-1 and AZO-2 sample.

The luminescence decay of AZO-1 and AZO-2 samples were measured for 523 nm emission under 375 nm excitation and are shown in Figure 7(b). It can be clearly seen that under UV excitation, the green emission in AZO-2 decays faster, the decay in AZO-1 is slower. However, careful curve fitting into multi -exponential equation with the expression of $I(t)= I_0+A_1 \exp(-t/\tau_1)+A_2 \exp(-t/\tau_2)$ reveal the difference in contribution of fast and slower decay components in each material. Table-2 enlists the decay parameters with their relative contributions in the photophysical process.

Table 2. Decay parameters of AZO-2 sample

Sample	τ_1 (μ sec) (Relative %)	τ_2 (μ sec) (Relative %)
AZO-1	0.58 (69%)	2.07 (31%)
AZO-2	0.35 (88%)	2.32 (12%)

Electrical transport properties like Seebeck and resistivity measurements revealed that both AZO-1 and AZO-2 shows n-type conduction owing to substitution of divalent Zn^{2+} ions with trivalent Al^{3+} ions forming shallow donor centers with excess electrons for conduction. The resistivity plot shown in Fig.8 (a) indicates that both AZO-1 and AZO-2 are showing metallic behavior over the whole measured temperature range, i.e. the resistivity increases with increasing temperature. Accordingly, the AZO-2 sample shows higher value of resistivity (1.03×10^{-3} ohm-m) at 300 K as compared to AZO-1 (1.01×10^{-3}), this increase in electrical resistivity of AZO-2 could be attributed to the formation of $ZnAl_2O_4$ and excess Zn vacancy in the presence of oxygen [25, 26].

The Zn^{2+} vacancies compensate for the free electrons in ZnO, thus enhances resistivity of AZO-2 as compared to AZO-1. The Seebeck coefficient (S) values of both AZO-1 and AZO-2 samples shown in Fig. 7(b) are negative over the whole examined temperature range, indicating n-type conduction. The absolute values of S of AZO-2 sample at room temperature (158.02 μVK^{-1}) is greater than AZO-1 sample (-172.5 μVK^{-1}) due to high temperature annealing of AZO-2 sample, which resulted in formation of additional cubic phase. leading to strong scattering from extended defects such as grain boundaries and $ZnO/ZnAl_2O_4$ interfaces.[27] The increase in carrier concentration causes a decrease in electrical resistivity leading to decrease in the value of Seebeck coefficient, (Pisarenko relation).

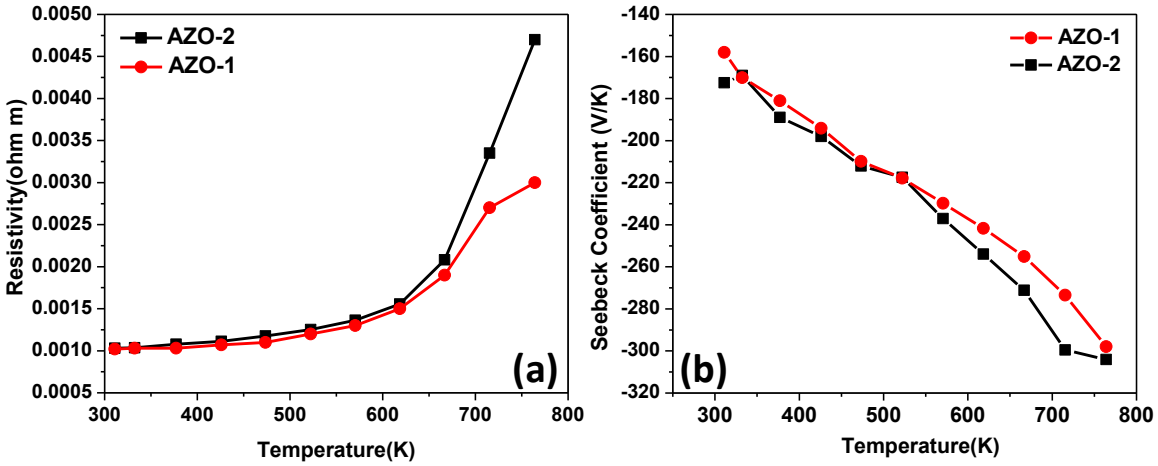

Fig.8. Variation of resistivity and Seebeck coefficient with temperature for AZO-1 and AZO-2 samples

The n-type conducting AZO-1 sample with better luminescent and electronic transport properties was used as a target for thin film deposition on quartz substrate. The resultant film was highly transparent in the visible region (400-700 nm) showing more than 80% transmittance. The transmission spectrum of the film is shown in Fig. 9.

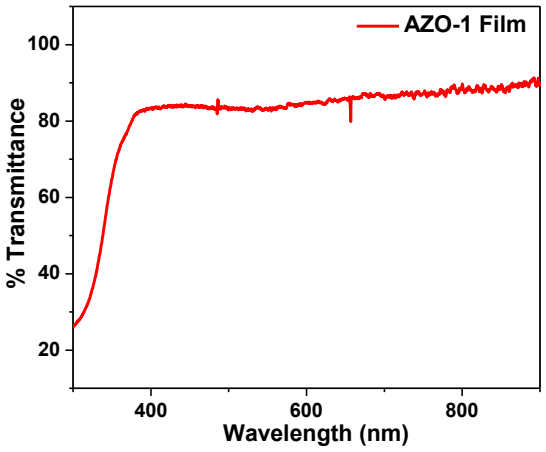

Fig 9. Transmission spectra of AZO-1 thin film on quartz substrate.

Conclusions

In summary, we report synthesis of highly luminescent and n-type conducting Al-doped ZnO (AZO) phosphors using flux-free solid-state reaction technique for fabrication of thin films. The precursor powders were pelletized and fired at 1000ºC (AZO-1). and 1200ºC (AZO-2) in a flowing O_2 gas environment by keeping the stabilization (dwell) time as 2 hours for all firings in the furnace. A new cubic phase (zinc aluminate) has been observed in the final compound after firing at 1200°C along with the wurtzite ZnO phase. The microstructure analysis was corroborated with Rietveld refinement studies on AZO-1 and AZO-2 samples. The photoluminescence (PL) measurements revealed that both AZO-1 and AZO-2 exhibited green (~523 nm) PL under UV (375 nm) excitation. It has been observed that the emission intensity of AZO-1 sample is comparatively higher than that of AZO-2 sample. The measurement of electronic transport properties of the AZO-1 and AZO-2 samples revealed their n-type behavior at room temperature (300 K), but the conductivity of AZO-1 is higher compared to AZO-2 due to scattering from various secondary phases present in the AZO-2 sample. The AZO samples have been used as target materials for transparent thin film deposition on quartz substrate, thus proving it to be ideal materials for solar cell applications.

Acknowledgements

This present work was supported by the CSIR-SRF program.

References

1. A. Ohtomo, K. Tamura, M. Kawasaki, T. Makino, Y. Segawa, Z. K. Tang, G. K. L. Wong, Y. Matsumoto, H. Koinuma, Applied Physics Letters 77 (14) (2000) 2204–2206.
2. Y. Z. Yoo, T. Fukumura, Z. Jin, K. Hasegawa, M. Kawasaki, P. Ahmet, T. Chikyow, H. Koinuma, Journal of Applied Physics 90 (8) (2001) 4246– 4250.
3. B. E. Sernelius, K. F. Berggren, Z. C. Jin, I. Hamberg, C. G. Granqvist, Phys. Rev. B 37 (17) (1988) 10244–10248
4. Z. Y Ning, S. H. Cheng, S. B. Ge, Y. Chao, Z. Q. Gang, Y. X. Zhang, Z. G. Liu., Thin Solid Films 50 (1997) 307
5. K. Postava, H. Sueki, M. Aoyama, T. Yamaguchi, K. Murakami, Y. Igasaki, Appl. Surf. Sci. 175 (2001) 543
6. T. Kojima, Phys. Status Solidi A 111 (1989) 233.
7. S. J. Pearton, D. P. Norton, K. Ip, Y. W. Heo, T. Steiner, Prog. Mater. Sci. 50 (2005) 293.
8. B. Claflin, D. C. Look, S. J. Park, G. Cantwell, Journal of Crystal Growth 287(1) (2006) 16–22.
9. A. Janotti, C. G. van de Walle, Phys. Rev. B. 76 (2007) 1–22
10. A. Janotti, G. van de Walle, Journal of Crystal Growth 287 (2006) 58–65
11. P. Jood, R. J. Mehta, Y. Zhang, G. Peleckis, X. Wang, R. W. Siegel, T. Borca-Tasciuc, S. Xue Dou, G. Ramanath, Nano Lett. 11 (2011) 4337–4342
12. A. Favier, D. Muñoz, S. Martín de Nicolás, P. -J. Ribeyron, Solar Energy Materials and Solar Cells 95 (2011) 1057–1061
13. V. Bhosale, J. T. Prater, F. Yang, D. Burk, S. R. Forrest, J. Narayan, J. Appl. Phys. 102 (2007) 1–5
14. N. Deng Pan, X. Tao, Z. Yu, L. Xiang Jun, Sci China Ser B-Chem 51 (2008) 823-828
15. R. Buonsanti, A. Llordes, S. Aloni, B. A. Helms D. J. Milliron, Nano Lett. 11 (2011) 4706–4710
16. S. Mondal, S. R. Bhattacharya, P. Mitra, J. Phys. 80 (2013) 2.
17. F. Maldonado, A. Stashans, J. Phys. and Chem. of Solids 17 (2010) 784-787
18. S. S. Lin, J. L. Huang, P. Šajgalik, Surf. Coat. Technol. 185 (2004) 254.
19. I. Miron , C. Enache and I. Grozescu, Digest Journal of Nanomaterials and Biostructures. 2012; 7:967-972.
20. Wei X and Chen D, Materials Letters. 2006; 60:823-827.
21. X. L. Wu, G. G. Siu, C. L. Fu, H. C. Ong, Appl. Phys.Lett. 78 (2001) 2285
22. N. Ohashi, T. Nakata, T. Sekiguchi, H. Hosono, M. Mizuguchi, T. Tsurumi, J. Tanaka, H. Haneda, Jpn. J. Appl.Phy. 38 (1999) 113.
23. X. L. Wu, G. G. Siu, C. L. Fu, H. C. Ong. Appl. Phys. Lett. 78 (2001) 2285
24. B. Lin, Z. Fu, Y. Jia, Appl. Phy. Lett. 79 (2001) 943
25. O. Lupan, S. Shishiyanu, V. Ursaki, H. Khallaf, L. Chow, T. Shishiyanu, V. Sontea, E. Monaico, S. Railean, Solar Energy Materials & Solar Cells. 93 (2009) 1417–1422
26. D. B´erardan, C. Byl and N. Dragoe, J. Am. Ceram. Soc. 93 (2010) 2352.
27. Y. Zhao, A. Kumar, G. A. Khodaparast, A. Eltahir, H. Wang and S. Priya, Energy Harvesting and Systems, 2014, DOI: 10.1515/ehs-2013–0024